SPATIAL DISTRIBUTION OF ENERGY DISSIPATION IN A TURBULENT CYLINDER WAKE

Jiangang Chen
Institute for Turbulence-Noise-Vibration Interactions and Control
Harbin Institute of Technology (Shenzhen)
Shenzhen 518055, China
chenjiangang@stmail.hitsz.edu.cn

Yu Zhou
Institute for Turbulence-Noise-Vibration Interactions and Control
Harbin Institute of Technology (Shenzhen)
Shenzhen 518055, China
yuzhou@hit.edu.cn

Robert Antonia
School of Engineering
University of Newcastle
NSW 2308, Australia
robert.antonia@newcastle.edu.au

Tongming Zhou
School of Civil, Environmental and Mining Engineering
The University of Western Australia
35 Stirling Highway, Crawley, WA 6009, Australia
tongming.zhou@uwa.edu.au

ABSTRACT

This work aims to improve our understanding of the turbulent energy dissipation rate in the turbulent wake of a circular cylinder. Ten of the twelve velocity derivative terms which make up the energy dissipation rate are simultaneously obtained with a probe composed of four X-wires. Measurements are made in the plane of mean shear at x/d = 10, 20 and 40, where x is the streamwise distance from the cylinder axis and d is the cylinder diameter, at a Reynolds number of 2.5×10^3 based on d and free-stream velocity. A phase-averaging technique is used to separate the coherent and remaining structures of the velocity derivatives and the energy dissipation rate $\overline{\varepsilon}$, approximated by a surrogate based on the assumption of homogeneity in the transverse plane. It is found that the velocity derivatives $\overline{(\partial u/\partial y)^2}$ and $\overline{(\partial v/\partial x)^2}$ play an important role in the interaction between large- and small- scale turbulent structures. The phase-averaged data indicate that energy dissipation occurs spatially mostly within the coherent spanwise vortices, rather than in the regions of turbulent mixing as described by in the widely accepted flow structure model (Hussain and Hayakawa, 1986, 1987). A revised model is proposed to reflect the present finding on the spatial distribution of the energy dissipation rate.

INTRODUCTION

The mean turbulent energy dissipation rate, which is of essential importance in small-scale turbulence study (e.g. Sreenivasan and Antonia, 1997) is given by

$$\begin{aligned}\overline{\varepsilon} &= \nu\overline{\frac{\partial u_i}{\partial u_j}\left(\frac{\partial u_i}{\partial u_j}+\frac{\partial u_j}{\partial u_i}\right)} \\ &= \nu\Big[\underbrace{2\overline{\left(\frac{\partial u}{\partial x}\right)^2}}_{1}+\underbrace{\overline{\left(\frac{\partial v}{\partial x}\right)^2}}_{2}+\underbrace{\overline{\left(\frac{\partial w}{\partial x}\right)^2}}_{3}+\underbrace{\overline{\left(\frac{\partial u}{\partial y}\right)^2}}_{4}+\underbrace{2\overline{\left(\frac{\partial v}{\partial y}\right)^2}}_{5}+\underbrace{\overline{\left(\frac{\partial w}{\partial y}\right)^2}}_{6} \\ &\quad+\underbrace{\overline{\left(\frac{\partial u}{\partial z}\right)^2}}_{7}+\underbrace{\overline{\left(\frac{\partial v}{\partial z}\right)^2}}_{8}+\underbrace{2\overline{\left(\frac{\partial w}{\partial z}\right)^2}}_{9}+\underbrace{2\overline{\frac{\partial u}{\partial y}\frac{\partial v}{\partial x}}}_{10}+\underbrace{2\overline{\frac{\partial u}{\partial z}\frac{\partial w}{\partial x}}}_{11}+\underbrace{2\overline{\frac{\partial v}{\partial z}\frac{\partial w}{\partial y}}}_{12}\Big]\end{aligned} \tag{1}$$

In Eq. (1), an overbar indicates a time-averaged quantity; ν is the kinematic viscosity; $u_{i,j}(\equiv \partial u_i/\partial x_j)$ is the derivative of velocity fluctuation u_i in the x_j direction, where i and j = 1, 2, and 3 represent the streamwise, lateral and spanwise directions, respectively, and are used interchangeably with x, y and z (figure 1).

Significant attention has been paid to the behaviour of $\overline{\varepsilon}$ in various flows. Browne et al. (1987) measured nine (1-9 in Eq. (1)) of the twelve terms of $\overline{\varepsilon}$ in a turbulent far wake (x/d = 420), and found that $\overline{\varepsilon}$ based on the isotropy assumption may underestimate the total dissipation rate by

45%-80% across the wake. Both George and Hussein (1991) and Mi and Antonia (2010) suggest that $\overline{\varepsilon}$ estimated based on the assumption of local axisymmetry is closer to the true value than that estimated based on the assumption of local isotropy in most turbulent shear flows.

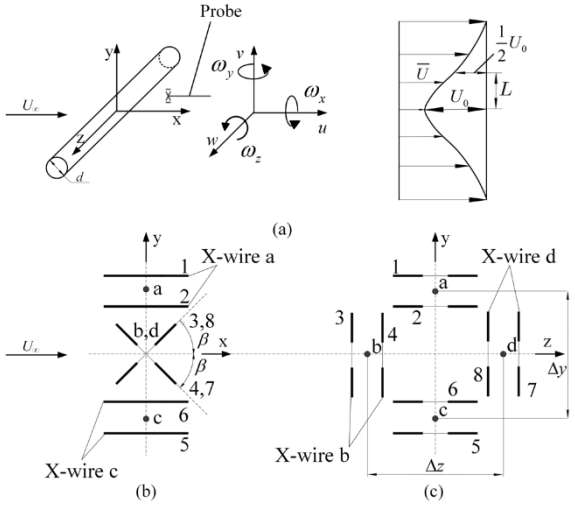

Figure 1. (a) Experimental arrangement, coordinate system, and definition sketch; (b) side view of the vorticity probe; (c) front view of the probe.

Zhu and Antonia (1996a) studied the correlation between enstrophy and energy dissipation rate in a turbulent wake with a four X-wire probe in the same shape as the probe used in the present study, and proposed an assumption of homogeneity in the transverse plane (*y*-*z* plane) of the wake. Based on this assumption, $\overline{(\partial v/\partial y)(\partial w/\partial z)} \approx \overline{(\partial v/\partial z)(\partial w/\partial y)}$. This has been recently validated by Lefeuvre et al. (2014) using direct numerical simulation (DNS) data in the intermediate wake of a square cylinder (x/d = 20 - 100). The sum of the unmeasured quantities $\overline{(\partial v/\partial y)^2}$ and $\overline{(\partial w/\partial z)^2}$ with the probe can therefore be estimated approximately as $\overline{(\partial u/\partial x)^2} - 2\overline{(\partial v/\partial z)(\partial w/\partial y)}$ using continuity and the approximation $\overline{(\partial v/\partial y)(\partial w/\partial z)} \approx \overline{(\partial v/\partial z)(\partial w/\partial y)}$. The mean energy dissipation rate based on the homogeneity in the transverse plane is then given by

$$\overline{\varepsilon}_{yz} = \nu\Big[4\Big(\overline{\Big(\frac{\partial u}{\partial x}\Big)^2} + \overline{\Big(\frac{\partial u}{\partial y}\Big)^2} + \overline{\Big(\frac{\partial u}{\partial z}\Big)^2} + \overline{\Big(\frac{\partial v}{\partial x}\Big)^2} + \overline{\Big(\frac{\partial v}{\partial z}\Big)^2} + \overline{\Big(\frac{\partial w}{\partial x}\Big)^2} + \overline{\Big(\frac{\partial w}{\partial y}\Big)^2}\Big) + 2\overline{\Big(\frac{\partial u}{\partial y}\Big)\Big(\frac{\partial v}{\partial x}\Big)} + 2\overline{\Big(\frac{\partial u}{\partial z}\Big)\Big(\frac{\partial w}{\partial x}\Big)} - 2\overline{\Big(\frac{\partial v}{\partial z}\Big)\Big(\frac{\partial w}{\partial y}\Big)}\Big] \quad (2)$$

Lefeuvre et al. (2014) compared various surrogates of $\overline{\varepsilon}$ based on different assumptions in the turbulent intermediate wake of a square cylinder, and found that $\overline{\varepsilon}_{yz}$ can provide the most accurate estimation of the energy dissipation rate. A similar result may be expected in the wake of a circular cylinder even though it may be less isotropic than a square cylinder wake (Antonia et al., 2002b). This expectation is not unreasonable since $\overline{\varepsilon}_{yz}$ contains nearly all the terms that make up the true energy dissipation rate in Eq. (1). Indeed, Eq. (2) has been used as the reference value of the true mean energy dissipation rate in quite a few studies (e.g. Zhu and Antonia, 1996a; Yiu et al., 2004; Mi and Antonia, 2010). Given that the detailed calibration of the present probe for measuring the velocity derivatives has been conducted in Antonia et al. (2002a), we take $\overline{\varepsilon}_{yz}$ as the reference value of $\overline{\varepsilon}$ in the present study.

Hussain and Hayakawa (1987) proposed a topological model for the mechanism of a turbulent plane wake, where the turbulence production occurs mainly along the diverging separatrix and the turbulent mixing takes place in the region where the ribs and rollers are in contact with each other. However, they provided no information on the spatial distribution of the turbulent energy dissipation in the model. Landau and Lifschitz (2011) commented that the energy dissipation rate had to be considered as a fluctuating quantity, in the same manner as any other fluctuating quantity which is likely to be affected by the large scale motions. A very distinct feature in a plane wake is the dominance of the Kármán vortex street at small x/d, which is followed by its gradual weakening and eventual disappearance as x/d increases. Therefore, it is of great importance and interest to investigate how the spatial organization of the turbulent energy dissipation rate is affected by the Kármán vortices and how this effect evolves downstream as the Kármán vortices weaken.

The present investigation focuses mainly on the characteristics of the energy dissipation rate in a turbulent cylinder wake (x/d = 10 - 40), special attention being given to its spatial distribution under the influence of the highly coherent Kármán vortices. A phase-averaging technique is used to separate the coherent structure and the remainder of the energy dissipation rate along with its components.

EXPERIMENTAL DETAILS

Experiments were conducted in an open-loop low turbulence wind tunnel with a working section of 0.35 m × 0.35 m and 2.4 m long. A circular cylinder with a diameter d = 12.7 mm was used to generate the wake. The free-stream velocity U_∞ = 3.0 m/s. The Reynolds number based on U_∞ and d is 2.5 × 10^3. A movable probe (figure 1b and c) consisting of four X-wires was used to measure the velocity fluctuations and their derivatives simultaneously. The separation between the two inclined wires of each X-wire was about 0.6 mm. Two of the X-wires, b and d, were aligned in the (x, y) plane and separated by Δz = 1.9 mm; the other two, a and c, were separated in the (x, z) plane by Δy = 1.9 mm. Measurements were made at x/d = 10, 20 and 40. The output signal from the anemometers were passed through buck and gain circuits and low-pass-filtered at a cur-off frequency f_c close to $\overline{U}_1/2\pi\eta$, which is commonly identified as the Kolmogorov frequency f_k, where $\overline{U}_1$ is the mean streamwise velocity on the centerline of the wake and $\eta \equiv (\nu^3/\overline{\varepsilon})^{1/4}$ is the Kolmogorov length scale. The filtered signal was subsequently sampled at a frequency $f_s = 2f_c$ (3200 Hz at x/d = 10 and 20; 2500 Hz at x/d = 40) using a 12-bit A/D converter. The record duration was about 60s.

Table 1 gives the maximum velocity defects U_0^*, wake half-width L^* and spatial resolution of the probe in terms of the Kolmogorov length scale at the wake centerline of

the local x^* position. Hereinafter, the asterisk '*' denotes the normalization by d and U_∞. The $\bar{\varepsilon}$ is estimated based on Eq. (2). The detailed description of the experimental set-up and estimation of the experiment uncertainty is available in Zhou et al. (2003) and will not be repeated here.

Table 1. Maximum velocity defect, mean velocity half-width and spatial resolution of the probe at the wake centreline of three x^* positions.

x^*	U_0^*	L^*	$\bar{\varepsilon}$	η	$\Delta x/\eta$	$\Delta y/\eta$	$\Delta z/\eta$
10	0.22	0.64	4.03	0.17	4.8	11.2	11.2
20	0.18	0.88	1.63	0.21	3.9	9.0	9.0
40	0.14	1.4	0.41	0.30	2.7	6.3	6.3

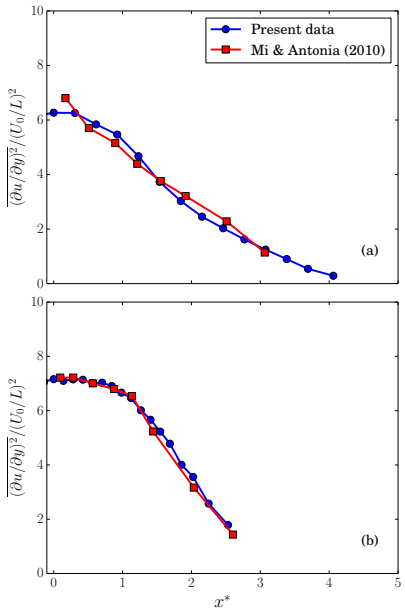

Figure 2 Comparison of $\overline{(\partial u/\partial y)^2}$ between the present data and those from Mi and Antonia (2010): (a) x^* = 10, (b) 40.

It is important to make sure that the spatial resolution of the probe is adequate for the study of the velocity derivatives and therefore the turbulent energy dissipation rate. Previous measurements indicated that the optimum wire separation of the probe for the velocity derivative measurement is about 3-5η (e.g. Antonia et al., 1993; Shafi and Antonia, 1997); a larger wire separation can cause the degraded velocity derivatives, while a smaller wire separation may overestimate the velocity derivatives because of the electronic noise contamination. The present vorticity probe was fabricated, with a great effort, to meet the above criterion of wire separation between the opposite two cross-wires, although the corresponding wire separations $\Delta y/\eta$ and $\Delta z/\eta$ (table 1) are still larger than the optimum value.

The attenuation of the spatial resolution of the probe is examined by comparing the distribution of $\overline{(\partial u/\partial y)^2}$ at x^* = 10 and 40 with those measured by Mi and Antonia (2010), as shown in figure 2. In their study of the local axisymmetry assumption for x^*=10 -70 (Re = 3000), they used two X-wires with a spatial resolution of about 8η at x^* =10 and 5 at x^*= 40, which are close to the optimum spatial resolution of about 4. In contrast, our spatial resolution is 11 at x^* = 10 and 6 at x^* = 40 (table 1). The agreement between the two sets of data actually is quite good, especially at x^* = 40. The present measurement appears to be appreciably below that of Mi and Antonia (2010) only near the centerline at x^* = 10 (y/L < 0.3). Zhu and Antonia (1996b) investigated the influence of the probe resolution on the spectra of vorticity measured using a probe with the same geometry used here. They found that the vorticity spectra were attenuated mainly at large wavenumbers. Note that the primary interest of the present study is the spatial distribution of the energy dissipation with respect to the Kármán vortices whose dimension is comparable to the wake half-width (Hussain and Hayakawa, 1987; Chen et al., 2016), much larger than the Kolmogorov length scale. As such, the resolution of the probe is considered to be adequate for the present study.

RESULTS AND DISCUSSION

In order to examine the spatial structure of the energy dissipation rate, a phase averaged technique is employed to separate the coherent structures from the remaining smaller scales of the flow field. The phase average of an instantaneous quantity Γ is given by $\langle\Gamma\rangle_p = \frac{1}{N}\sum_{i=1}^{N}\Gamma_{p,i}$, where p represents phase and N is the total number of detections, about 1800, 1700 and 400 at x^* = 10, 20 and 40, respectively. Based on the triple decomposition (Hussain 1983), Γ can be viewed as the sum of the time mean component $\overline{\Gamma}$ and the fluctuating component γ. The latter can be further decomposed into a coherent fluctuation $\tilde{\gamma}$ and a remainder γ_r, viz. $\gamma = \tilde{\gamma} + \gamma_r$. The $\tilde{\gamma} \equiv \langle\gamma\rangle$ is connected to the large-scale coherent structures, while γ_r is the remainder.

Hereinafter, the phase ϕ in the iso-contour plot will be interpreted in terms of a longitudinal distance based on Taylor's hypothesis, ϕ = 0 to 2π corresponding to the averaged vortex wavelength. The same scale is used for the longitudinal and lateral directions in the contour plots in an effort to minimize any possible distortion in the physical space. The positions of the centers and saddle points, identified from the phase-averaged sectional streamlines (not shown), are marked by '+' and '×', respectively. The thick dashed lines give an approximate idea of the periphery of the spanwise vortex, which is about 25% of the maximum magnitude of $\tilde{\omega}_z$ (not shown). The inclined dash dotted line passing through the saddle point represents the diverging separatrix. Flow is from left to right.

Figure 3 shows the phase-averaged iso-contours of two predominant components, $(\widetilde{\partial u/\partial y}^*)^2$ and $(\widetilde{\partial v/\partial x}^*)^2$, of the energy dissipation rate at x^* = 10 and 40, their maximum concentrations being one order of magnitude larger

than those of the other components. This is not surprising since $(\widetilde{\partial u/\partial y}^*)^2$ and $(\widetilde{\partial v/\partial x}^*)^2$ are associated with the coherent spanwise vorticity $\widetilde{\omega_z}^*(=\widetilde{\partial v/\partial x}^* - \widetilde{\partial u/\partial y}^*)$. At x^* = 10 (figure 3a, c), the concentration of $(\widetilde{\partial u/\partial y}^*)^2$ occurs near the border of the vortex, while that of $(\widetilde{\partial v/\partial x}^*)^2$ coincides approximately with the vortex center. There is a phase shift of about $\pi/2$ between the maximum concentrations of $(\widetilde{\partial u/\partial y}^*)^2$ and $(\widetilde{\partial v/\partial x}^*)^2$. The different behaviors of the two quantities reflect largely the distinct influence of the anisotropic large-scale motion on different velocity derivatives. At x^* = 40 (figure 3b, d), the phase shift between the maximum concentrations of $(\widetilde{\partial u/\partial y}^*)^2$ and $(\widetilde{\partial v/\partial x}^*)^2$ shrinks as the Kármán vortices become weak due to, e.g., breaking up (Chen et al., 2016). Note that the maximum concentration of $(\widetilde{\partial u/\partial y}^*)^2$ is about 2-3 times that of $(\widetilde{\partial v/\partial x}^*)^2$ at the two x^* positions, which is ascribed to the influence of mean shear $(\overline{U}/\partial y)$.

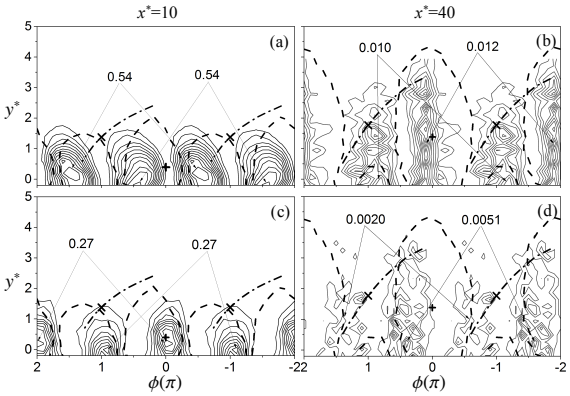

Figure 3. Iso-contours of the phase-averaged velocity derivatives (a, b) $(\widetilde{\partial u/\partial y}^*)^2$ and (c, d) $(\widetilde{\partial v/\partial x}^*)^2$. Contour interval: (a-d) 0.049, 0.0013, 0.030, 0.0010.

The iso-contours of $\langle(\partial u/\partial y)_r^2\rangle^*$and $\langle(\partial v/\partial x)_r^2\rangle^*$, which are in general associated with the remaining smaller-scale motions, are similarly distributed, with their maximum concentrations within the spanwise vortex at x^* = 10 (figure 4a, c) but appear disorganized at x^* = 40 (figure 4b, d) probably due to the very weak Kármán vortices there. In distinct contrast to the large disparity in the magnitude of the maximum concentration between $(\widetilde{\partial u/\partial y}^*)^2$ and $(\widetilde{\partial v/\partial x}^*)^2$ (figure 3), the maximum $\langle(\partial u/\partial y)_r^2\rangle^*$ and $\langle(\partial v/\partial x)_r^2\rangle^*$ are quite close to each other, even at x^* = 10 where the coherent motions are strong. In fact, the iso-contours of the remainders for other velocity derivatives (not shown) also display similar topologies to those of $\langle(\partial u/\partial y)_r^2\rangle^*$ and $\langle(\partial v/\partial x)_r^2\rangle^*$ at the same x^*, with comparable maximum concentrations. This is reasonable since the small-scale structures of the velocity derivatives are expected to be more isotropic compared to the large-scale structures, even under the influence of the relatively strong coherent motions at x^* = 10.

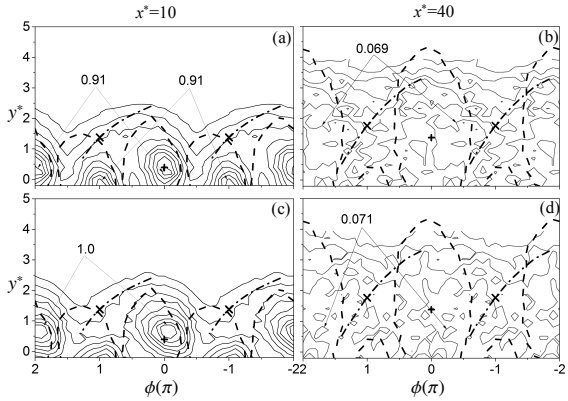

Figure 4. Iso-contours of the remainders (a, b) $\langle(\partial u/\partial y)_r^2\rangle^*$ and (c, d) $\langle(\partial v/\partial x)_r^2\rangle^*$. Contour interval: (a-d) 0.10, 0.010, 0.11, 0.013.

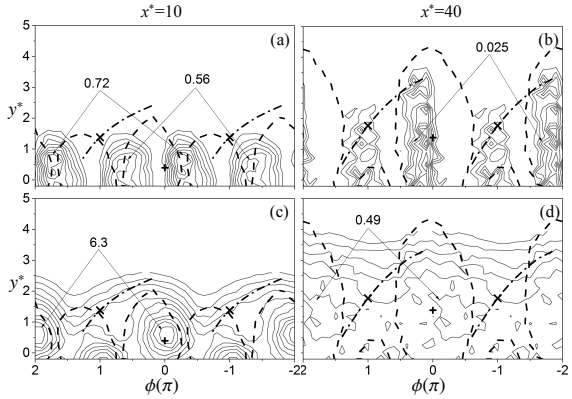

Figure 5. Iso-contours of the phase-averaged turbulent energy dissipation rate (a, b) $\widetilde{\varepsilon_{yz}}^*$ and the remainder (c, d) $\langle\varepsilon_{yz,r}\rangle^*$. Contour interval: (a-d) 0.080, 0.0028, 0.57, 0.072.

Figure 5 presents the iso-contours of the phase-averaged energy dissipation rate $\widetilde{\varepsilon_{yz}}^*$ and the remainder $\langle\varepsilon_{yz,r}\rangle^*$ at x^* = 10 and 40. The iso-contours (figure 5a, b) of the coherent energy dissipation rate exhibit a distribution similar to $(\widetilde{\partial u/\partial y}^*)^2$ (figure 3a, b), which makes the predominant contribution to $\widetilde{\varepsilon_{yz}}^*$. On the other hand, the concentrations of the remainder (figure 5c, d) coincide very well with the Kármán vortex, as those of $\langle(\partial u/\partial y)_r^2\rangle^*$ and $\langle(\partial v/\partial x)_r^2\rangle^*$ (figure 4), particularly at x^* = 10 and x^* = 20 (not shown). The maximum concentration of $\widetilde{\varepsilon_{yz}}^*$ (0.72, 0.025 at x^* = 10 and 40, respectively) is much smaller than that of the corresponding remainder (6.3, 0.49) because energy dissipation occurs primarily at small scales (e.g. Pope 2001). It seems plausible that the turbulent energy dissipation takes place predominantly within the Kármán vortices, at least for $x^* \le 20$. The observation of the remainder energy dissipation rate is consistent with Hussain and Hayakawa's (1987) finding that the incoherent turbulence intensity occurs largely within the Kármán vortex at x^* = 10 - 40 and its maximum concentration almost coincides with the Kármán vortex center. Since the turbulent energy dissipation rate physically reflects the rate of the turbulent energy dissipated into heat at small scales, its

spatial distribution is expected to be associated with that of the remainder or small-scale turbulent energy. At $x^* = 10$, the Kármán vortices are strong and highly organized; as such, the iso-contours of the energy dissipation rate appear to be well organized (figure 5a, c). At $x^* = 40$ (figure 5b, d), the Kármán vortices are very weak due to vortex interactions and breakup. As a result, the coherent energy dissipation rate appears markedly less organized; so does the remainder. Nevertheless, the maximum concentration of the remainder remains discernible within the Kármán vortex periphery.

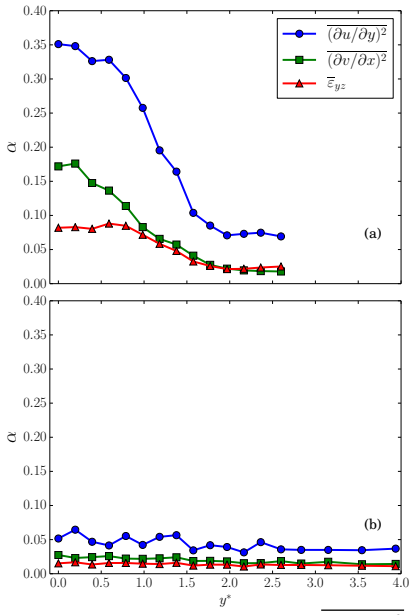

Figure 6. Coherent contributions (α) to $\overline{(\partial u/\partial y)^2}$, $\overline{(\partial v/\partial x)^2}$ and $\overline{\varepsilon}_{yz}$ across the wake at $x^* =$ (a) 10, (b) 40.

The well-organized structures at $x^* = 10$, as evident in the iso-contours of $(\widetilde{\partial u/\partial y}^*)^2$ and $(\widetilde{\partial v/\partial x}^*)^2$ (figure 3) and $\widetilde{\varepsilon}^*_{yz}$ (figure 5) are apparently correlated with the occurrence of the Kármán vortices. The effect of the large-scale motion on the small scales can be quantified by the coherent contribution, which is given at a given y^* position by the ratio of the structural average of the phase-averaged coherent quantity to the corresponding Reynolds-averaged quantity (Zhou et al. 2003), namely

$$\alpha = \overline{\widetilde{\beta}\widetilde{\gamma}}/\overline{\beta\gamma} \qquad (3)$$

where β and γ represent the velocity derivatives $\partial u_i/\partial x_j$, and the double bar means average within one vortex shedding period.

Figure 6 presents the distribution of α of $\overline{(\partial u/\partial y)^2}$, $\overline{(\partial v/\partial x)^2}$ and $\overline{\varepsilon}_{yz}$ across the wake at $x^* = 10$ and 40. The coherent contribution to the mean energy dissipation, i.e. $\overline{\widetilde{\varepsilon}_{yz}}/\overline{\varepsilon}_{yz}$, is calculated as the ratio to $\overline{\varepsilon}_{yz}$ of the sum of the structural average of all the terms making up $\overline{\varepsilon}_{yz}$ in Eq. (2).

At $x^* = 10$ (figure 6(a)), the coherent contribution accounts for $\overline{(\partial u/\partial y)^2}$ and $\overline{(\partial v/\partial x)^2}$ up to 35% and 18%, respectively, near the centerline. Such large coherent contributions are internally in agreement with the well organized structures of their coherent part at $x^* = 10$ (figure 3a, c).

The maximum coherent contribution to $\overline{\varepsilon}_{yz}$ is about 9% at $y^* = 0.6$ which roughly corresponds to the y^* position of the maximum concentration of $\widetilde{\varepsilon}^*_{yz}$ (figure 5a). This relatively small contribution compared with that to $\overline{(\partial u/\partial y)^2}$ or $\overline{(\partial v/\partial x)^2}$ is mainly from $\overline{\overline{(\widetilde{\partial u/\partial y})^2}}$ and $\overline{\overline{(\widetilde{\partial v/\partial x})^2}}$, and the coherent contributions from the other velocity derivative terms to $\overline{\varepsilon}_{yz}$ are all quite small. The results suggest that the coherent motions make a large contribution to $\overline{(\partial u/\partial y)^2}$ and $\overline{(\partial v/\partial x)^2}$, though the coherent contribution to the total energy dissipation rate is small, which intrinsically reflects the way how the small scales feel the influence from the large-scales associated with the Kármán vortices. It seems that the large-scale coherent motions of the present flow interact with the small-scale turbulence mostly via $\partial u/\partial y$ and $\partial v/\partial x$. The effect of the large-scale motions can be still felt at $x^* = 20$ (not shown), where the maximum coherent contribution to $\overline{(\partial u/\partial y)^2}$, $\overline{(\partial v/\partial x)^2}$ and $\overline{\varepsilon}_{yz}$ are about 15%, 6% and 4%, respectively. Because of the rather weak coherent motions at $x^* = 40$, the coherent contribution there is negligibly small (figure 6b).

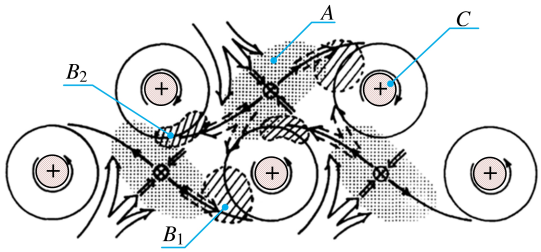

Figure 7. Topological model of flow in a plane wake. +, vortex centre; ×, saddle point; ⇒ engulfed non-turbulent fluid; ==> flow of produced turbulence; A: turbulence production; B1 & B2: turbulent mixing; C: turbulent kinetic energy dissipation.

Hussain and Hayakawa (1987) proposed a topological model for explaining the mechanisms of the turbulent plane wake. Since the energy dissipation rate was not measured, the model did not provide any information on the spatial distribution of the energy dissipation rate. Figures 5 shows unequivocally that the predominant turbulent energy dissipation rate, i.e. $\langle \varepsilon_{yz,r} \rangle^*$, is mostly concentrated within the spanwise vortex, particularly at $x^* = 10$, which should be ascribed to the high concentration of turbulent kinetic energy there (Hussain and Hayakawa 1987). As a result, a more complete picture may be cast presently for the turbulence dynamics by incorporating the information on the energy dissipation rate into Hussain and Hayakawa's model, as shown in figure 7. The saddle region (denoted as A), where intense strain is induced by the rotating motion of successive vortices, can be identified with the turbulent energy production area. The non-

turbulent fluid from the free stream is engulfed into the rotating motion of the ribs (or quasi-streamwise vortices) and is subjected to the vortex stretching by the strain along the diverging separatrix, leading to the production of turbulence. Turbulent mixing would mostly occur at the region (denoted as B1 and B2) where the streamwise vortex and the spanwise vortex are in contact with each other since the direct interaction between the two near orthogonal vortex structures can produce three-dimensional vorticity fluctuations (Hussain and Hayakawa 1987). The turbulence thus produced will then be entrained by the rotational motion of the spanwise vortex and accumulated within the vortex structure before being finally dissipated as flow develops downstream.

CONCLUSIONS

(1) It is found that $\overline{(\partial u/\partial y)^2}$ and $\overline{(\partial v/\partial x)^2}$ play an important role in the interaction between large-scale and small-scale motions in the present flow. The maximum coherent contribution associated with the Kármán vortices to $\overline{(\partial u/\partial y)^2}$ and $\overline{(\partial v/\partial x)^2}$ can be as high as 35% and 18%, respectively, near the centerline at $x^* = 10$; on the other hand, the coherent contributions to the other velocity derivatives are almost one order of magnitude smaller, resulting in a maximum coherent contribution to the total mean energy dissipation rate of about 9% at $x^* = 10$. Thiesset et al. (2014) found that, close to the wake generator (say at $x^* = 10$), the influence of the coherent motions can be felt by even the smallest scales. The present study further indicates that the coherent motions in the present flow interact with the small-scale turbulence mostly via $\partial u/\partial y$ and $\partial v/\partial x$.

(2) Iso-contours of the phase-averaged energy dissipation rate $\widetilde{\varepsilon}_{yz}$ are quite similar to those of $(\widetilde{\partial u/\partial y})^2$ which contributes most to $\widetilde{\varepsilon}_{yz}$. The concentrations of the remainder $\langle \varepsilon_{yz,r} \rangle$, whose maximum is nearly one order of magnitude larger than that of $\widetilde{\varepsilon}_{yz}$, occur mainly within the Kármán vortices. It is concluded that the dominating energy dissipation takes place within the Kármán vortex. A more complete picture for the flow mechanism is thus proposed by incorporating the information on the energy dissipation into Hussain and Hayakawa's model, as shown in figure 7.

ACKNOWLEDGEMENT

YZ wishes to acknowledge support given to him from NSFC through grant 11632006 and The National Research Foundation for the Doctoral Program of Higher Education of China under Grant No. 20132302110054.

REFERENCES

Antonia R. A., Orlandi P., Zhou T., 2002a, "Assessment of a three-component vorticity probe in decaying turbulence", *Experiments in Fluids* Vol. 33, pp. 384–390.

Antonia R. A., Zhou T. M., Romano G. P., 2002b, "Small-scale Turbulence Characteristics of Two-dimensional Bluff Body Wakes", *Journal of Fluid Mechanics*, Vol. 459, pp. 67–92.

Antonia R. A., Zhu Y., Kim J., 1993, "On The Measurement of Lateral Velocity Derivatives in Turbulent Flows", *Experiments in Fluids*, Vol. 15, pp. 65–69.

Browne L., Antonia R. A., Shah D. A., 1987, "Turbulent Energy Dissipation in a Wake", *Journal of Fluid Mechanics*, Vol. 179, pp. 307–326.

Chen J. G., Zhou Y., Zhou T. M., Antonia R. A., 2016, "Three-dimensional Vorticity, Momentum and Heat Transport in a Turbulent Cylinder Wake", *Journal of Fluid Mechanics,* Vol. 809, pp. 135–167.

George W., Hussein H., 1991, "Locally Axisymmetric Turbulence", *Journal of Fluid Mechanics,* Vol. 233, pp.1–23.

Hussain A. K. M. F., 1983, "Coherent Structures—Reality and Myth", *Physics of Fluids*, Vol. 26, pp. 2816.

Hussain A. K. M. F., 1986, "Coherent structures and turbulence", *Journal of Fluid Mechanics*, Vol. 173, pp. 303-356.

Hussain A. K. M. F., Hayakawa M., 1987, "Eduction of Large-scale Organized Structures in a Turbulent Plane Wake", *Journal of Fluid Mechanics*, Vol. 180, pp. 193-229.

Landau L. D., Lifschitz E. M. (2011) "Fluid Mechanics", Elsevier/Butterworth Heinemann, Amsterdam.

Lefeuvre N., Thiesset F., Djenidi L., Antonia R. A. , 2014, "Statistics of the Turbulent Kinetic Energy Dissipation Rate and Its Surrogates in a Square Cylinder Wake Flow", *Physics of Fluids,*Vol. 26, pp. 95104.

Mi J., Antonia R. A., 2010, "Approach to Local Axisymmetry in a Turbulent Cylinder Wake", *Experiments in Fluids,* Vol. 48, pp. 933–947.

Pope S. B., 2001, "Turbulent Flows", *Cambridge University Press*, Cambridge, New York

Shafi H. S., Antonia R. A., 1997, "Small-scale Characteristics of a Turbulent Boundary Layer Over a Rough Wall", *Journal of Fluid Mechanics,* Vol. 342, pp. 263–293.

Sreenivasan K. R., Antonia R. A., 1997, "The Phenomenology of Small-scale Turbulence", *Annual Review of Fluid Mechanics,* Vol. 29, pp. 435–472.

Thiesset F., Danaila L., Antonia R. A., 2014, "Dynamical Interactions Between the Coherent Motion and Small Scales in a Cylinder Wake", *Journal of Fluid Mechanics,* Vol. 749, pp. 201–226.

Yiu M. W., Zhou Y., Zhou T., Cheng L., 2004, "Reynolds Number Effects on Three-Dimensiional Vorticity in a Turbulent Wake", *AIAA Journal,* Vol. 42, pp. 1009–1016.

Zhou T., Zhou Y., Yiu M. W., Chua L. P., 2003, " Three-dimensional Vorticity in a Turbulent Cylinder Wake", *Experiments in Fluids,* Vol. 35, pp. 459–471.

Zhu Y., Antonia R. A., 1996a, "On the Correlation Between Enstrophy and Energy Dissipation Rate in a Turbulent Wake", *Applied Scientific Research,* Vol. 57, pp. 337–347.

Zhu Y., Antonia R. A., 1996b, "Spatial Resolution of a 4-X-wire Worticity Probe", *Measurement Science Technology,* Vol. 7, pp. 1492.